

12-11-2014

A 3D Kinematic Study of the Northern Ejecta 'Jet' of the Crab Nebula

Christine S. Black
Dartmouth College

Robert A. Fesen
Dartmouth College

Follow this and additional works at: <https://digitalcommons.dartmouth.edu/facoa>



Part of the [Astrophysics and Astronomy Commons](#)

Recommended Citation

Black, Christine S. and Fesen, Robert A., "A 3D Kinematic Study of the Northern Ejecta 'Jet' of the Crab Nebula" (2014). *Open Dartmouth: Faculty Open Access Articles*. 1825.
<https://digitalcommons.dartmouth.edu/facoa/1825>

This Article is brought to you for free and open access by Dartmouth Digital Commons. It has been accepted for inclusion in Open Dartmouth: Faculty Open Access Articles by an authorized administrator of Dartmouth Digital Commons. For more information, please contact dartmouthdigitalcommons@groups.dartmouth.edu.

A 3D KINEMATIC STUDY OF THE NORTHERN EJECTA “JET” OF THE CRAB NEBULA

CHRISTINE S. BLACK & ROBERT A. FESEN

6127 Wilder Lab, Department of Physics & Astronomy, Dartmouth College, Hanover, NH 03755

Draft version April 8, 2018

ABSTRACT

We present moderate resolution [O III] $\lambda\lambda 4959, 5007$ line emission spectra of the Crab Nebula’s northern ejecta jet. These data along with an [O III] image of the Crab Nebula were used to build 3-dimensional kinematic maps of the jet and adjacent remnant nebulosity to better understand the jet’s properties and thus its likely origin. We find the jet’s systemic velocity to be $+170 \pm 15$ km s⁻¹ with radial velocities ranging from -190 to $+480$ km s⁻¹. Our data indicate that the jet consists of thin filamentary walls ($V_{exp} \simeq 40 - 75$ km s⁻¹), is virtually hollow in [O III] emission, and elliptical and funnel-like in shape rather than a straight cylindrical tube as previously thought. Examination of the Crab’s 3D filamentary structure along the jet’s base reveals a large and nearly emission-free opening in the remnant’s thick outer ejecta shell. The jet’s blueshifted and redshifted sides are surprisingly well defined and, like the jet’s sharp western limb, appear radially aligned with the remnant’s center of expansion. These alignments, along with the opening in the nebula at the jet’s base and proper motions indicating an expansion age in line with the 1054 supernova event, suggest a direct connection between the jet’s formation and the Crab’s radial expansion. While our analysis supports the scenario that the jet may simply represent the highest velocity material of the remnant’s N-S bipolar expansion, the nature of this expansion asymmetry remains unclear.

Subject headings: Crab Nebula, supernova remnant

1. INTRODUCTION

The Crab Nebula was the first supernova remnant to be associated with a “guest star” seen by ancient Chinese and Japanese astronomers in 1054 AD (Hubble 1928; Lundmark 1938; Duyvendak 1942), the first pulsar firmly associated with a supernova remnant (Comella et al. 1969; Cocke et al. 1969) as well as the first astronomical object found to emit synchrotron radiation (Shklovskii 1953, 1957; Dombrovski 1954). Despite being one of the best studied astronomical objects, a few properties of the Crab have not yet been fully understood (see reviews by Davidson & Fesen 1985, Hester 2008, and Bühler & Blandford 2014).

One of these is the nature of a curious filamentary feature 45'' wide and extending approximately 100'' off the nebula’s northern limb. First reported as a “faint jetlike structure” seen in deep optical images by van den Bergh (1970), narrow pass-band optical images showed it consists of line emitting filaments which are brightest in [O III] $\lambda\lambda 4959, 5007$ (Chevalier & Gull 1975; Gull & Fesen 1982). Subsequent deep radio and optical continuum studies showed the presence of associated extremely faint synchrotron emission (Velusamy 1984; Woltjer & Veron-Cetty 1987).

Follow-up spectral and kinematic studies show the feature to be hollow (Fesen & Gull 1983; Shull et al. 1984), with a mean radial velocity expansion of 260 km s⁻¹, and a mean heliocentric velocity of 184 km s⁻¹ (Marcelin et al. 1990). It also appears to be slightly tilted into the plane of the sky by eight degrees (Shull et al. 1984) and, although large in extent, has a relatively small estimated mass $\approx 0.003 M_{\odot}$ (Veron-Cetty et al. 1985).

A particularly interesting but puzzling aspect of this feature is its parallel edge morphology making it appear more like a cylinder rather than a diverting outflow of radially expanding ejecta. While its sharp western edge closely aligns back to the Crab’s estimated center of expansion (Fesen & Gull 1986; Fesen & Staker 1993), its central axis is unaligned

with either the center of expansion or the remnant’s pulsar. Although sometimes referred to as a ‘trail’, ‘spur’, ‘stem’, or ‘chimney’ (Blandford et al. 1983; Kundt 1983; Morrison & Roberts 1985), here we will use the word ‘jet’ as it was originally described by van den Bergh (1970), but this should not be taken as necessarily implying a narrow or directed beam of material or energy.

A variety of explanations have been proposed to explain the nature of the Crab’s jet (see Table 1). One early theory involved a two-component pulsar wind nebula (PWN) model where dense, line radiation emitting filaments were frozen in a “strong” 10⁻³ Gauss magnetic field. Field lines forced between the filaments via plasma instabilities then expand outward forming the jet (Bychkov 1975; Marcelin et al. 1990). Other models suggest a combination of magnetic fields and the Crab’s PWN leading to a Rayleigh-Taylor instability ‘bubble’ bursting through the nebula’s shell of ejecta (Chevalier & Gull 1975; Sankrit & Hester 1997).

While some theories invoke instabilities within the Crab’s structure to describe the formation and uniqueness of the jet, alternative hypotheses suggested that the ambient interstellar medium (ISM) surrounding the nebula contributed to the jet’s formation. In these models, the jet’s formation was attributed to Rayleigh-Taylor instabilities in the remnant’s shell of filaments that result as the remnant expanded into a low density region in the local ISM (Kundt 1983; Veron-Cetty et al. 1985).

Other proposals include a relativistic plasma beam resulting from magnetic fields directly off the pulsar (Shull et al. 1984; Benford 1984; Michel 1985; Bietenholz & Kronberg 1990) or that the jet is just the highest velocity component of the Crab’s N-S bipolar expansion (Fesen & Staker 1993; Rudie et al. 2008). A mass-loss trail from the red giant progenitor star was proposed by Blandford et al. (1983), and Morrison & Roberts (1985) suggested that it was formed as a result of the interaction between a small local interstellar cloud creating a ‘shadowed flow’.

TABLE 1
PROPOSED EXPLANATIONS FOR THE JET'S FORMATION

Theory	References
Filaments in Expanding Magnetic Field	Bychkov (1975); Marcelin et al. (1990)
PWN Driven Instability and Breakout	Chevalier & Gull (1975); Sankrit & Hester (1997); Smith (2013)
Mass-loss Trail from Red Giant Progenitor	Blandford et al. (1983)
Expansion into a Low Density ISM Region	Kundt (1983); Veron-Cetty et al. (1985)
Relativistic Pulsar Beam	Shull et al. (1984); Benford (1984)
	Michel (1985); Bietenholz & Kronberg (1990)
Interaction with a Local Interstellar Cloud	Morrison & Roberts (1985)
Highest-Velocity Ejecta of N-S Bipolar Expansion	Fesen & Staker (1993); Fesen et al. (1997); Rudie et al. (2008)

In order to explore its kinematic properties as a means of better constraining its likely origin, we obtained moderate dispersion, long slit spectra of its [O III] line emission. These data allow us to investigate in detail the jet's kinematic structure in relation to the main nebula along the Crab's northern limb and whether the jet's structure is connected to the Crab's expansion point. Our observations are described in §2, our results and 3-dimensional reconstructions presented in §3, our analysis in §4, our discussion of the results in §5, and our conclusions in §6.

2. OBSERVATIONS

Optical spectra of the Crab's northern jet feature were taken in October 2013 with the 2.4m Hiltner telescope at the MDM Observatory on Kitt Peak, AZ using a Boller and Chivens CCD Spectrograph (CCDS) and a 1800 grooves mm^{-1} grating blazed at 4700 Å yielding 0.275 Å per pixel. A $1''.2 \times 264''$ N-S slit was placed along the jet's western edge with the bottom of the slit approximately $50''$ above the center of expansion as defined by Nugent (1998) (J2000) $05^{\text{h}}34^{\text{m}}32.84^{\text{s}} +22^{\circ} 00' 48''.0$).

Fourteen 900s spectra were taken covering the width of the jet, moved approximately $5''$ between each exposure. The slit positions are shown in Figure 1. The resulting spectra have a FWHM resolution of 0.7 \AA ($\approx 40 \text{ km s}^{-1}$) and covered 330 \AA which included $\text{H}\beta$ and [O III] $\lambda\lambda 4959, 5007$ and a scale of $0''.363 \text{ pixel}^{-1}$. Velocity measurements are believed accurate to $\pm 15 \text{ km s}^{-1}$ for all but the faintest jet emission features. Comparison spectra for wavelength calibration were taken using the Ar, Hg, Ne, and Xe lamps. Data reduction was done using IRAF¹ and consisted of bias and background subtraction, wavelength calibration, and cosmic ray removal.

3. ANALYSIS

A 3-dimensional kinematic representation of the jet was constructed using the jet's [O III] $\lambda\lambda 4959, 5007$ emission lines. Due to the nebula's expansion velocity reaching as high as 1800 km s^{-1} (Lundqvist & Tziamtzis 2012), a portion of the most blueshifted $\lambda 5007$ emissions overlapped with the most redshifted $\lambda 4959$ emissions. This $\lambda 4959$ emission line overlap was removed by assuming a $I(5007)/I(4959)$ ratio of 2.91 (Osterbrock & Ferland 2006). Figure 2 shows an example of the reduced data.

A 2005 Subaru [O III] image of the Crab Nebula (Fig. 1; see Rudie et al. 2008) was used to match the jet's features

with those seen in the spectra. This image along with an assumed distance for the Crab of $d_2 = 2.0 \pm 0.5 \text{ kpc}$ (Trimble 1968, 1973), a formation date of 1054 AD for the jet based on its measured proper motions (Rudie et al. 2008), and the center of expansion determined by Nugent (1998) were used to calculate the transverse velocities for features in the jet.

Due to its faintness, we divided the jet into two different regions for analysis: the jet's base comprising the interface of it with the Crab's northern limb, and the jet feature itself. Code developed in Python was used to create a 3D map of the jet (from its base to the farthest extent northward) while the Crab Nebula's northern limb and jet interface was mapped using an IDL code and covered the region from the jet's base down well into the Crab's interior. For the purposes of this work, the dividing line between these two regions was defined as the northern most star of the double stars seen along the jet's southwestern limb (J2000) $05^{\text{h}}34^{\text{m}}31.68^{\text{s}} +22^{\circ} 03' 29''.61$; see Fig. 1).

The jet's emission structure was subdivided into eight sections as shown in Figure 3. We use the notation SXX to indicate the distance in arcsec each section is above the base of the jet. Each jet section is roughly $7''$ thick except for S96 which is $18''$ thick due the faintness of features near the jet's northern tip.

The jet's lower and top ring sections (S0 and S96) were excluded from parts of our kinematic analysis of the jet structure since they were either too contaminated by the main nebula or too sparsely populated. The remaining six rings (S14, S28, S40, S50, S65, and S78) were used to determine the expansion properties of the jet.

Our kinematic analysis of the jet's emission structure was developed using the *matplotlib* libraries within Python. Data from each slit were represented by a sample of points selected by eye along the jet's filamentary structure. The total sample contained over 2,700 points in an effort to faithfully map the jet's filamentary structure as well as provide a representation of intensity along the features. This method has the added benefit of removing any stellar continuum from the map. With the construction of this 3D map, features like the western and eastern walls could be isolated, analyzed, and viewed from various angles giving a better understanding of the jet's overall structure.

A 3D map of [O III] emission at the jet – nebula interface was constructed by creating a data array from the 14 slit spectra using the IDL subroutine VOLUME. Only pixels with intensities at least three times that of the background were used. Dark lines running through the resulting 3D image are the stellar continua of stars detected within the slits.

¹ IRAF is distributed by the National Optical Astronomy Observatories, which are operated by the Association of Universities for Research in Astronomy, Inc., under cooperative agreement with the National Science Foundation.

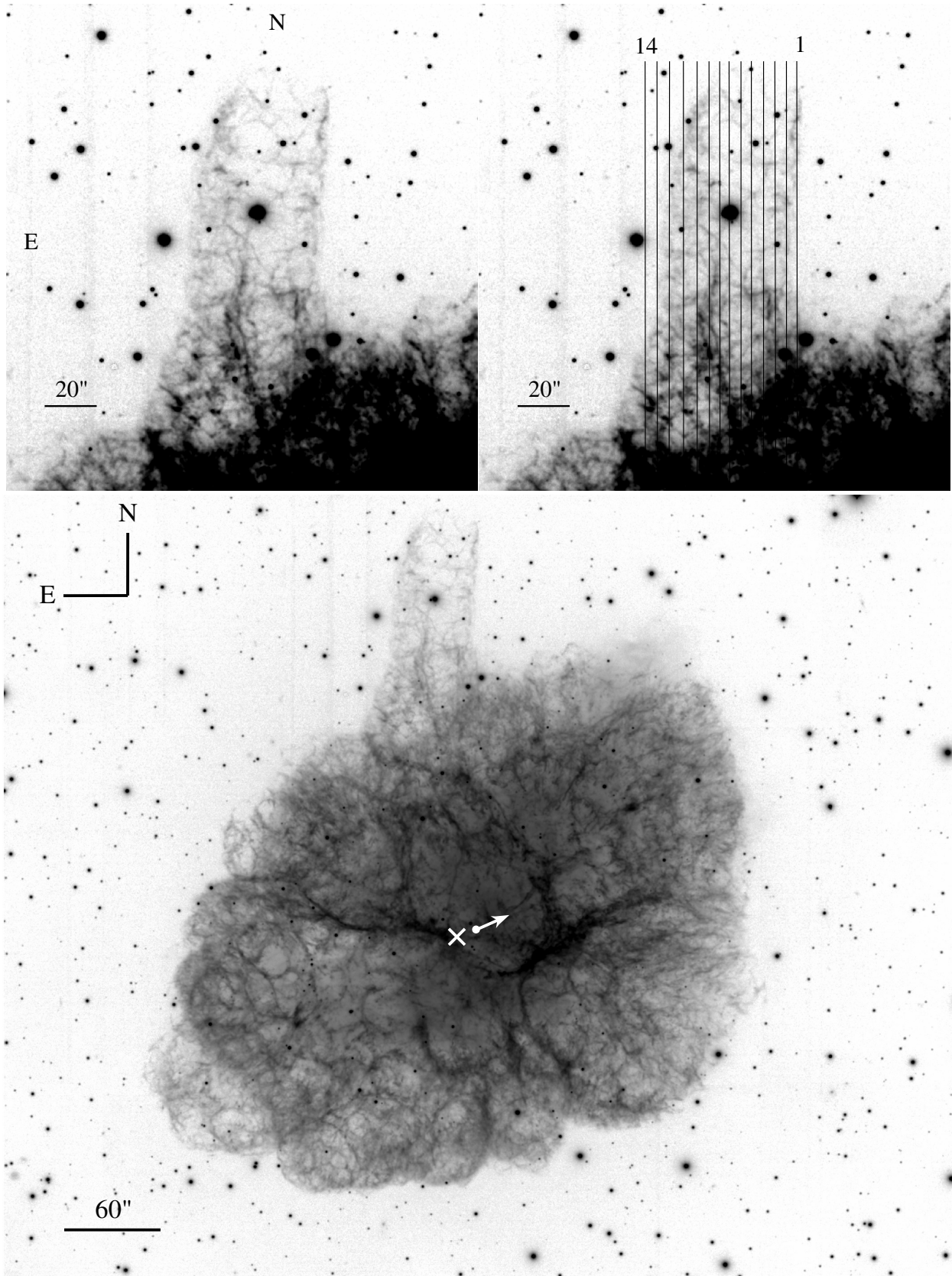


FIG. 1. — A 2005 [O III] $\lambda 5007$ image of the Crab Nebula's northern ejecta "jet" (upper left panel) from Rudie et al. (2008) with the 14 north-south slit positions overlaid (upper right panel). Bottom panel: Image of the whole Crab Nebula showing the northern jet with respect to the entire remnant. The 'X' marks the Nugent (1998) center of expansion and the white dot and arrow marks the pulsar and its proper motion direction as determined by Kaplan et al. (2008).

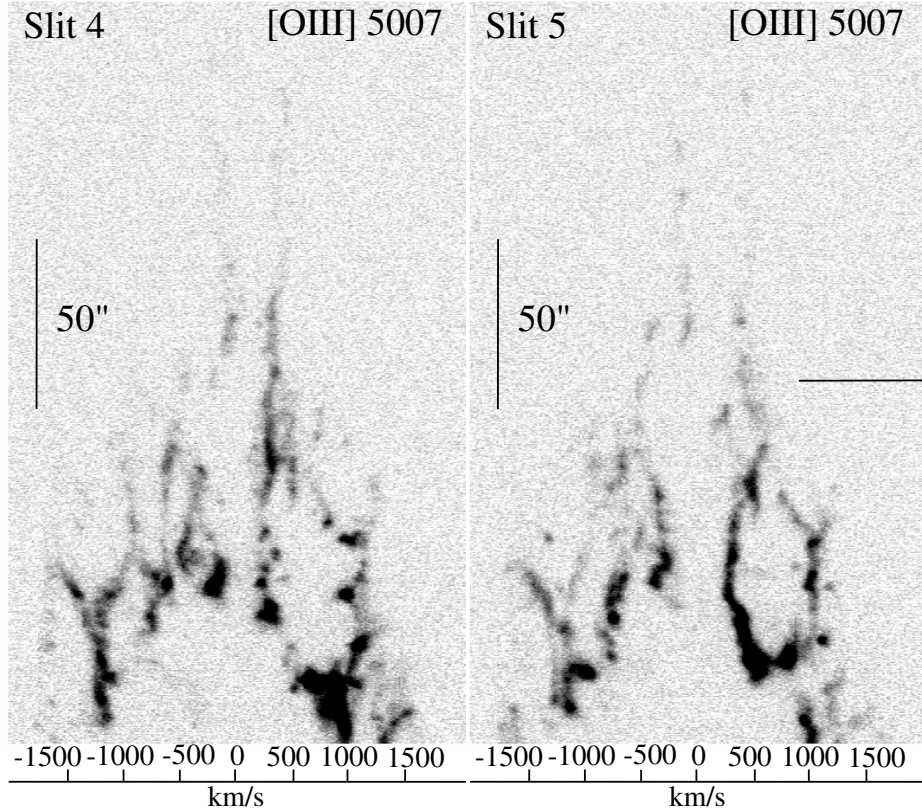


FIG. 2.— Spectra for slit positions 4 and 5 showing the $\lambda 4959$ subtracted $\lambda 5007$ [O III] line emission structure. In the right panel, the horizontal line marks the base of the jet.

4.1. Jet Morphology

Figure 4 shows the eight individual jet sections plotted in terms of radial velocity (V_R) and east-west transverse velocity ($V_T(\alpha)d_2$) relative to the remnant's expansion point (Nu-

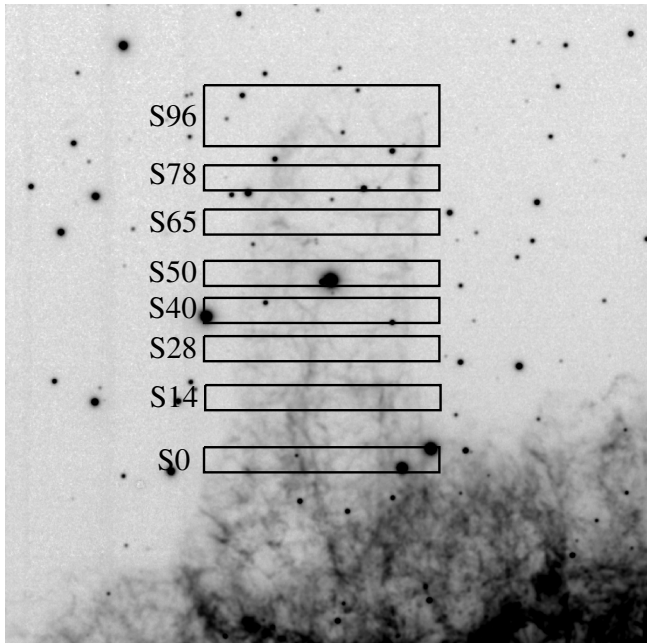


FIG. 3.— Positions of our selected jet sections.

gent 1998) where the sections are offset to give the portion of the jet directly above the nebula's center of expansion zero radial velocity. The sections S0, S14, S28, S40, S50, S65, S78, and S96 are color coded as purple, violet, blue, cyan, green, orange, maroon, and red, respectively.

With the exception of the most southern section (S0) near the base of the jet, these plots show the jet's structure to be remarkably empty of [O III] emission with well defined ring-like structures. While adjacent jet sections exhibit fairly similar appearances and dimensions, moving from just above the jet's base (S14) to its northern tip (S96), these rings of [O III] emission become larger in diameter but also less complete. This gradient in diameter can easily be seen, for example, by comparing S28 (blue) to S78 (maroon) or S14 (violet) to S96 (red).

In contrast, the lowest jet section, S0, shows no single distinct ring of emission, instead consists of several small cavities between filaments. This sort of small-scale, bubble-like morphology is present throughout the remnant so its appearance here in section S0 which includes the northern limb of the Crab's thick ejecta shell is not unexpected. However, the apparent lack of a hole in the S0 section coincident with the emission rings seen in the upper jet sections is misleading since even extremely faint emissions are plotted here, thus giving the appearance of a more filled structure.

Figure 4 also shows the jet's filamentary walls to be relatively thin compared to the jet's ≈ 650 km s^{-1} radial velocity range. We note that apparent narrowness of some ring sections in transverse velocity is due in some measure to the limited slit coverage of our data. Nonetheless, we find the jet

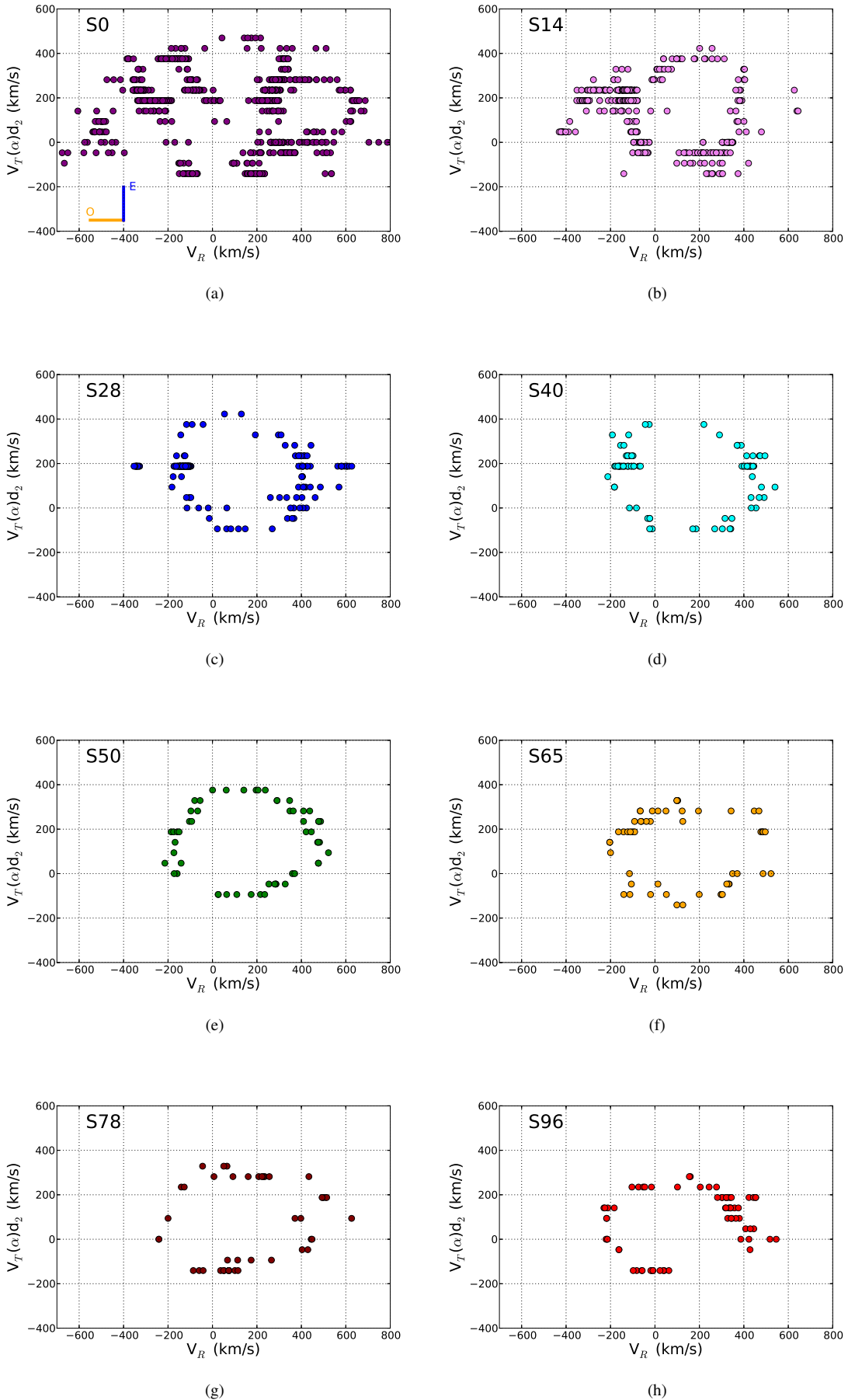


FIG. 4.— Velocity plots for our eight chosen jet sections shown in Figure 3 where V_R is the radial velocity and $V_T(\alpha)d_2$ is the east–west transverse velocity using a distance, d , of 2 kpc. (a) S0 (b) S14 (c) S28 (d) S40 (e) S50 (f) S65 (g) S78 (h) S96. A color version of this figure is available in the online journal.

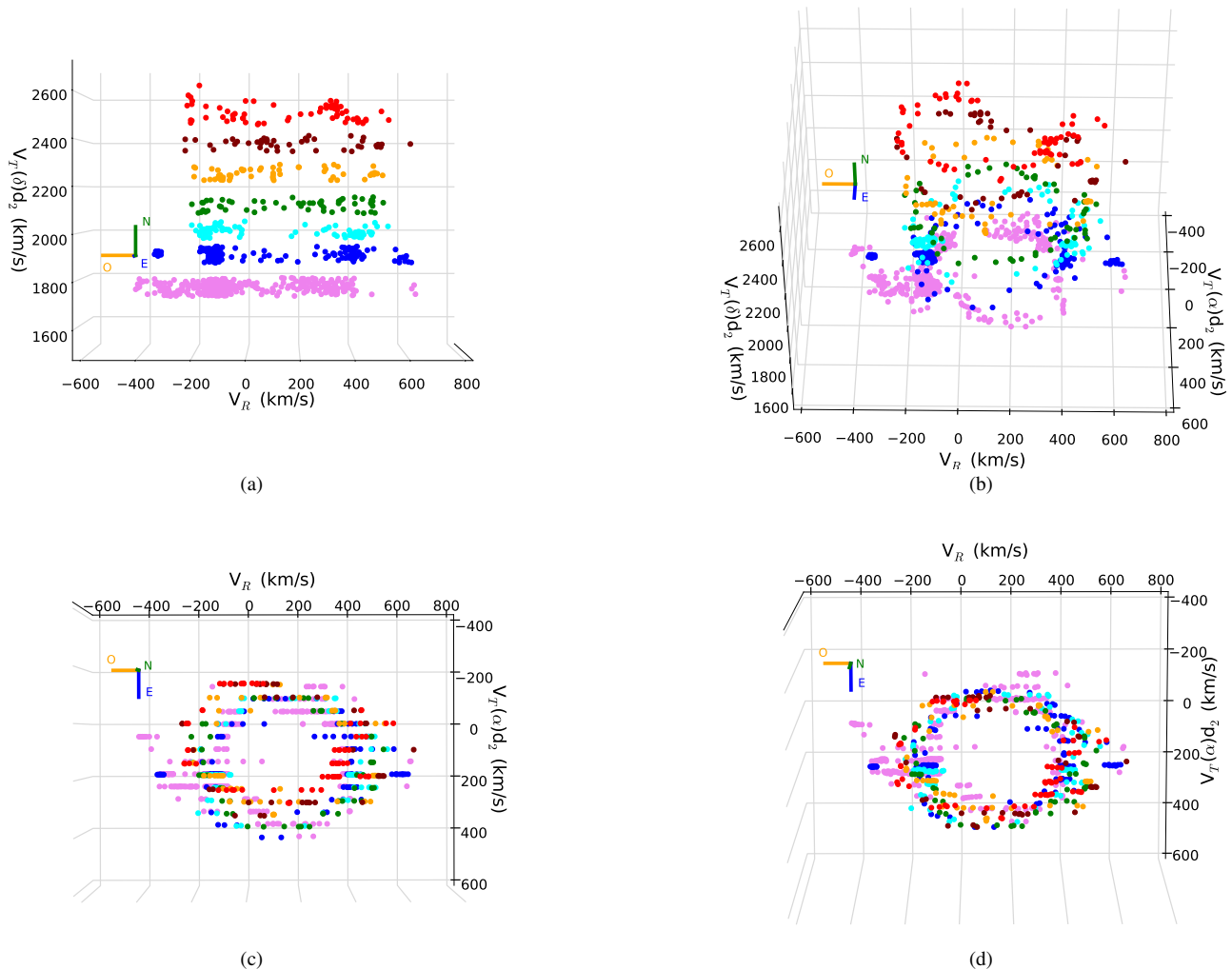


FIG. 5.— Combined velocity plots of the seven upper sections (S14 in violet to S96 in red) of the Crab jet viewed at angles of: (a) 0° , (b) 45° , (c) 90° , and (d) 100° . A color version of this figure is available in the online journal.

walls to have a typical thicknesses of $\simeq 40 - 75 \text{ km s}^{-1}$, consistent with an estimate of 60 km s^{-1} reported by Marcelin et al. (1990) based on lower dispersion data. However, there are several exclusions to this range in certain ring sections where jet walls can exceed a 100 km s^{-1} range in velocity.

Fewer [O III] filaments are present farther up the jet especially along its northeastern limb. Consequently, its upper northernmost sections becomes less complete. This incompleteness can be seen as gaps in the top three ring sections (S65, S78, and S96) of the jet. The largest of these missing sections is in the topmost ring (S96) which coincides with the highly curved appearance of the jet along its northeastern tip.

Previous studies of the Crab jet found the jet to be cylindrical in shape (Gull & Fesen 1982; Marcelin et al. 1990) as its near parallel limb shape might indicate. However, our 3D mapping suggests that the jet is actually elliptical in shape and increasingly so farther up the jet ($e \simeq 0.1 - 0.4$) with its major axis pointed nearly in to the plane of the sky (position angle $\simeq 340^\circ$) as can be seen in the individual sections shown in Figure 4.

In Figure 5, we show the upper seven jet sections when viewed from four different angles; 0, 45, 90, and 100 degrees. These plots highlight the jet’s slightly elliptical shape, its rela-

tively well defined walls, and the east-west transverse velocity offset from the remnant’s center of expansion.

As the viewing angle is increased, one is increasingly looking down the jet’s major axis. At a viewing angle of 100° degrees, the seven ring sections appear nearly aligned and the jet is seen as virtually hollow of [O III] emission. We estimate the jet’s angle of inclination into the plane of the sky (redshifted) to be roughly 10 ± 2 degrees, a bit more than the previous estimate of eight degrees by Shull et al. (1984).

4.2. Radial Velocities

The average velocities of the most redshifted, most blueshifted, and east and west sides for the middle six jet ring sections are listed in Table 2. Measured jet section velocities were averaged to minimize bias caused by our approach of using increased data points to simulate the jet’s brighter features. The maximum blueshifted and redshifted velocities were used to find the jet’s systemic heliocentric velocity which we estimate to be $+170 \pm 15 \text{ km s}^{-1}$.

The expansion velocities listed in Table 2 reveal a few interesting kinematic properties of the jet. First, radial velocities of the jet’s eastern limb remain relatively constant with the exception near the top of the jet where the filaments become

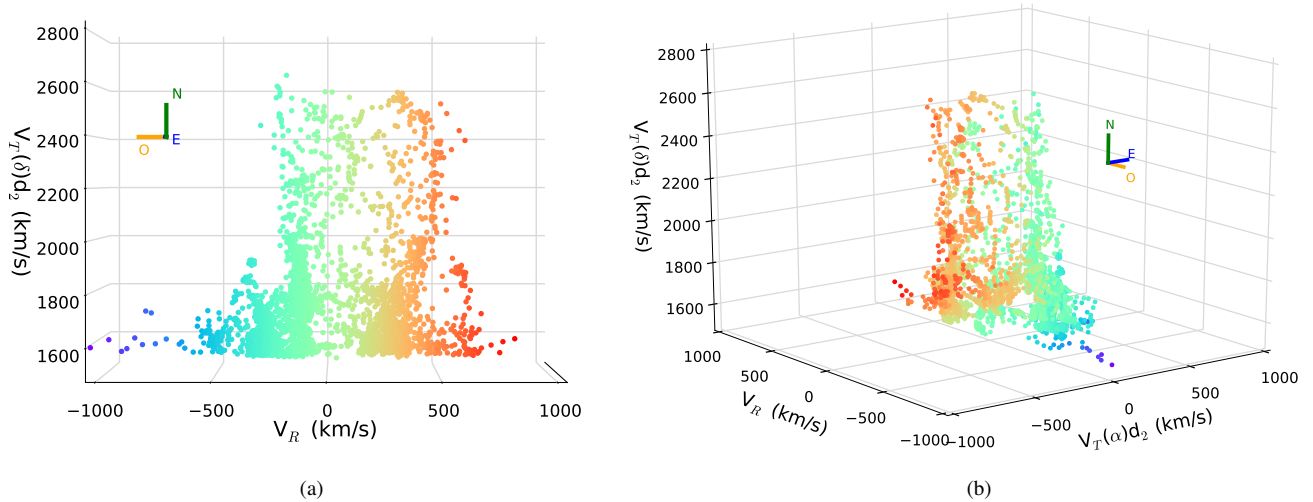


FIG. 6.— 3-dimensional views of the Crab Jet. Red to blue colors correspond to positive and negative radial velocities, respectively. (a) Side view of jet. (b) Angled view from front of jet. As in Figure 4, V_R represents radial velocity while $V_T(\alpha)d_2$ and $V_T(\delta)d_2$ are the transverse velocities in RA and Dec using a distance, d , of 2 kpc. ‘O’ is the direction to the observer, ‘N’ and ‘E’ are the North and East directions on the sky. A color version of this figure is available in the online journal.

TABLE 2
RADIAL VELOCITIES OF THE JET RING SECTIONS

Jet Section	Blue side (km/s)	Red side (km/s)	East Limb (km/s)	West Limb (km/s)
S78 (Maroon)	-190	+480	+150	+100
S65 (Orange)	-180	+480	+160	+140
S50 (Green)	-170	+475	+175	+195
S40 (Cyan)	-170	+460	(+100)	+195
S28 (Blue)	-160	+440	+170	+200
S14 (Purple)	-145	+415	+170	+205

NOTE. — Radial velocities accurate to ± 15 km/s

more sparse. This velocity continuity suggests that the jet’s eastern limb is fairly uniform despite an appearance of being less straight and well defined than the jet’s western limb. The radial velocities of the east and west limbs of S40, specifically the east limb, are smaller than expected due to a gap in the ring section which can be seen in Figure 4(d).

In contrast, radial velocities along the jet’s west limb decrease from around +200 to +100 km s⁻¹ from the bottom ring S14 to the upper ring S78 suggesting it is tilted less into the sky plane than the east limb.

More significant is the change in radial velocities of the redshifted and blueshifted sides from the jet’s bottom (S14) to the top (S78). The velocities slowly increase from the base of the jet to its top and a slight increase in the size of the rings follows this pattern as well. This increase in radii is visible in Figure 5 but more easily seen in Figure 4. The observed change in velocities over the length of the jet shows the jet possesses an opening, funnel-like shape rather than being a simple, straight walled cylinder as its projected parallel edge shape on the sky would indicate.

Figure 6 shows our 3D maps with all emission features plotted, not just those within our eight jet sections. Red to blue colors correspond to measured positive to negative radial velocities. Two viewing angles of the jet are shown with ‘O’ being the direction of the observer and ‘N’ and ‘E’ are the

North and East directions on the sky.

From the base to about the middle of the jet, there is a noticeable gradient of increasing radial velocity. The top of the redshifted side curves toward lower velocities, but this should not be mistaken as a cap at the top of the jet.

The plots in Figure 6 show that, with the exception of a handful of points, the jet’s blueshifted side is surprisingly well defined and sharply edged starting at a N-S transverse velocity ($V_T(\delta)d_2$) of 1800 km s⁻¹ up to and including 2600 km s⁻¹. In addition, lower down in the jet from $V_T(\delta)=1800$ to 2000 km s⁻¹ a majority of blueshifted jet features are aligned in parallel with this edge.

In contrast, the jet’s redshifted rear side is not as nearly well defined as its blueshifted side. Nonetheless, a number of features at the jet’s base show an angled alignment, although not parallel with the upper redshifted jet regions.

4.3. Correlation to The Remnant’s Center of Expansion

It has long been realized that the jet’s straight western limb is roughly aligned back to the Crab’s center of expansion (Morrison & Roberts 1985; Fesen & Gull 1986; Fesen & Staker 1993). This situation led us to examine if the front and rear sides of the jet seen in our 3D maps might also show some alignment back to the Crab’s center of expansion.

Figure 7 plots all our measured jet features along with the Crab’s estimated expansion point (Nugent 1998). The blue and red lines shown are drawn from the maximum blueshifted and redshifted portions of section S96 back toward the center of expansion. As can be seen, these lines appear in approximate alignment with the jet’s front (blue) and rear (red) sides.

Of course, there is significant uncertainty inherent in determining such alignments. The jet is, after all, composed of diffuse filaments and emission knots and the jet’s walls are not perfectly sharply defined. Nonetheless, one finds good alignment on the facing, blueshifted side but poorer on the rear, redshifted side. The fact that one sees some alignment at all between the jet’s walls and the projections from the Crab’s expansion center, when taken together with a similar alignment

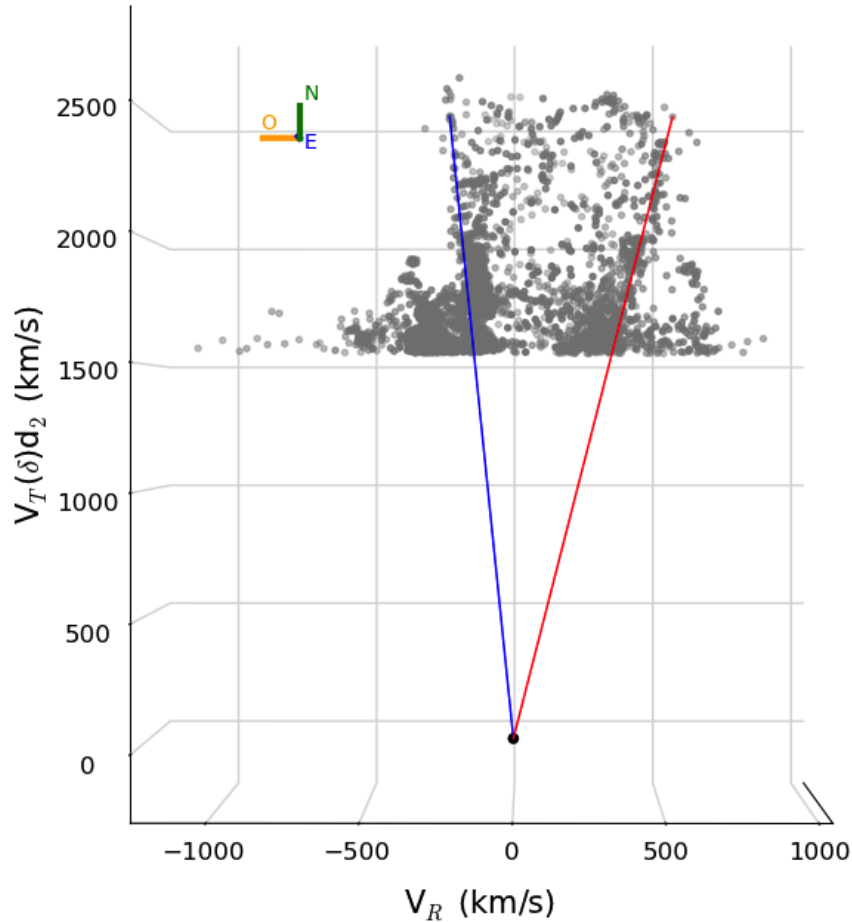


FIG. 7.— Plot of jet knots and filaments with respect to the Crab Nebula’s expansion center. Again, V_R and $V_T(\delta)d_2$ denote radial and transverse velocities respectively. A color version of this figure is available in the online journal.

of the jet’s western limb, lends support to radially expanding jet formation models.

4.4. Jet-Nebula Interface

Drifted scanned averaged spectra of the Crab Nebula taken with N-S aligned slits have long shown that the remnant’s expansion is strongly asymmetric, resembling a N-S bipolar expansion, with the lowest expansion velocities seen near an east-west belt of exceptional He-rich filaments (MacAlpine et al. 1989; Fesen et al. 1997; Smith 2003; Satterfield et al. 2012). The jet’s location along the Crab’s northern limb places it near the top of this bipolar expansion.

Such low-dispersion scanned spectra suggested a possible opening or channel in the nebula’s thick ejecta shell at the northern extreme of this bipolar structure and near the base of the jet (see Fig. 6 in Fesen et al. (1997)). We have used our higher resolution 3D map of the [O III] emission at the jet’s base and the remnant’s northern limb to investigate this possible shell break at the jet/nebula interface region.

The left hand panel of Figure 8 shows the [O III] $\lambda\lambda 4959, 5007$ and $H\beta$ line emission profiles from a N-S slit scanned in the east-west direction across the inner 2 arcmin section of the Crab obtained by Fesen et al. (1997). Like that seen in similar scanned spectra taken by MacAlpine et al. (1989) and Smith (2003), this spectrum shows a systematic velocity decrease or ‘pinching’ near the remnant’s central zone in both [O III] and

$H\beta$, coincident with the remnant’s bright central filaments. Toward the top of the northern (upper) expansion bubble, the spectra indicate a possible partial break in an otherwise thick, unbroken shell of emission filaments. In contrast, no similar break or channel appears present in the southern expansion bubble.

The right hand panel of Figure 8 shows our 3D reconstruction of the [O III] emission in this region using only slits 4 through 8. Unlike the scanned spectra seen in the left hand panel which shows no break in the northern expansion bubble, our 3D mapping reveals a long and fairly distinct area nearly devoid of [O III] emission. Several emission features defining this channel can also be seen in the lower resolution scanned long-slit spectra. The opening in this channel is much clearer in our data and this difference is presumably due to the wider 2 arcmin coverage of the scanned long slit data as compared to our 3D mapping which was both more limited in area and centered on the jet.

Although largely empty, a few faint filaments lie at the northern end of this channel and connect with emission seen at the base of the jet and visible in jet ring section S0 shown in Figure 4a. The channel’s walls connect to the jet’s base at the northernmost limb of the nebula.

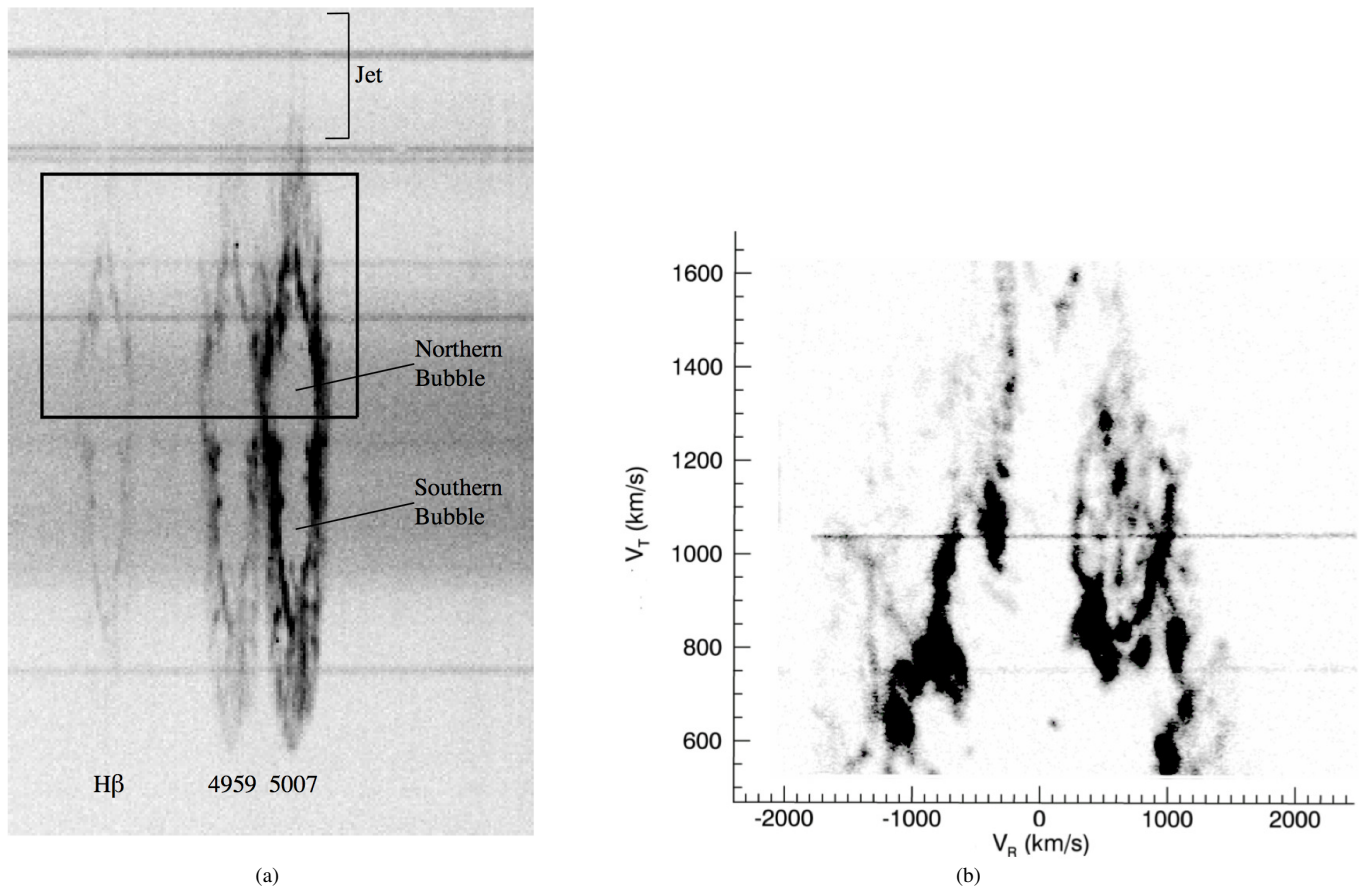


FIG. 8.— (a) [O III] $\lambda\lambda 4959, 5007$ and $H\beta$ line emissions from a scanned spectrum of the Crab using a N-S slit (Fesen et al. 1997). (b) Our 3D map of the Crab Nebula from the bottom of the slit to the base of the jet using slits 4-8. The box marks the N-S extent of our slit positions used to create the 3D map of the jet-nebula interface. Note: The dark horizontal lines are stellar continua.

Although it has been over three decades since the jet was first detected and its peculiar morphology recognized, its origin and nature has remained uncertain. Our new spectroscopic data provides a higher resolution view of the jet’s kinematic structure than previous studies, thus offering new insights and constraints regarding its possible origin.

Despite a striking, parallel tube-like appearance, our 3D mapping shows that the jet is actually elliptical in shape and wider at the top than its base, indicative of a funnel-like structure. This funnel-like structure is not likely the result of lateral expansion due to the synchrotron nebula within the jet because little, if any, synchrotron emission is seen near the top of the jet. The approximate alignment of the jet’s blue and redshifted sides with the Crab’s center of expansion is consistent with proper motion measurements of individual jet knots and filaments which show it to be radially expanding with an age matching that of the Crab’s supernova explosion date (Fesen & Staker 1993; Rudie et al. 2008).

Our spectral reconstruction of the jet’s interface with the Crab’s thick filamentary shell revealed a significant hole or ‘channel’ largely free of [O III] emission that was only hinted in earlier low dispersion N-S scanned spectra of the Crab (Fig. 8). The walls of this cavity are closely aligned with the walls of the jet suggesting a direct connection between the jet’s formation and this opening in the Crab’s northern limb.

Taken together, the jet’s hollow and funnel-like structure, the radial alignment of its western limb and blueshifted front side back to the Crab’s center of expansion, an age consistent

with the 1054 supernova event, and its location above a gap in the Crab’s emission shell disfavor certain proposed theories of the jet’s origin. Its radial motions appear inconsistent with a RGB mass-loss trail and pulsar beaming models, and models involving interaction with a local gas cloud near the supernova does not explain the jet’s lack of emission at its base.

On the other hand, theories of the jet’s origin involving the pulsar wind nebula (PWN) leading to instabilities in the filamentary shell, or a faster expansion of filaments due to a low density region in the surrounding ISM would appear consistent with the jet’s kinematic and emission properties discussed above. The presence of synchrotron emission in the jet (Wilson & Weiler 1982; Velusamy 1984) lends further support to PWN instability breakout models (Chevalier & Gull 1975; Sankrit & Hester 1997; Smith 2013).

However, breakouts of the PWN seen elsewhere along the Crab’s outer boundary do not show any entrained filamentary emission similar to that seen for the northern jet. Examples of synchrotron emission outside the remnant’s sharp [O III] emission boundary can be seen along northwest and west limbs of the Crab in the optical (see our Fig. 1; Fesen et al. 1992; Tziamtzis et al. 2009; Loll et al. 2013) and radio (Wilson et al. 1985). In addition, PWN instability breakout models do not make any prediction regarding the jet’s northern limb location especially given its position so far off the NW/SE axis of the pulsar’s wind nebula (Hester et al. 2002; Ng & Romani 2004; Kaplan et al. 2008).

In contrast, the transition from the Crab’s northern expan-

sion ‘bubble’ into the channel that leads up to the jet as shown in Figure 8 suggests that if the northern bubble is a result of the initial expansion post-supernova, the channel and jet are causally related to the supernova event as well. This conclusion is consistent with the jet’s radial proper motions and funnel-like shape with walls pointing back towards the Crab’s center of expansion. A simple explanation for the jet’s formation is that it is the highest velocity component of the Crab’s N-S bipolar expansion.

If this picture is correct, it then suggests that the Crab’s expansion was confined to some significant degree in most other directions. The source of this confinement could be the progenitor’s expected super-AGB mass loss wind as discussed by Sollerman et al. (2001) and Moriya et al. (2014). Based upon the jet’s maximum velocity, this confinement of the Crab’s expansion would seem fairly significant. Whereas nebula filaments along the northern limb of the Crab exhibit transverse velocities around $1600 \text{ d}_2 \text{ km s}^{-1}$, the location of the jet’s northernmost tip implies a transverse velocities around $2650 \text{ d}_2 \text{ km s}^{-1}$. This means that if the jet is part of the north bipolar flow, it extends the northern expansion bubble velocity by 1000 km s^{-1} .

Although direct images give the impression the jet arises northward out from the Crab’s northern limb, this is not precisely correct. The heliocentric systemic velocity of the Crab is low and effectively 0 km s^{-1} ($-20 \pm 50 \text{ km s}^{-1}$ Clark et al. 1983, $-55 \pm 35 \text{ km s}^{-1}$ Davidson 1987, $+1$ to -7 km s^{-1} Wallace et al. 1999). Thus, our estimated $+170 \text{ km s}^{-1}$ systemic velocity of the jet means that it is located on the remnant’s rear hemisphere, and tilted some 10 degrees back into the sky plane.

Moreover, the jet’s displacement to the east from the center of expansion means that spectra resulting from east-west scans of the remnant using N-S long slits are then not strictly aligned with the central axis of the Crab’s bipolar expansion. Therefore, such spectral scans give an imperfect view of the remnant’s expansion morphology.

In any case, the nature of the remnant’s apparent N-S bipolar expansion, of which the jet lies at the northern tip of, remains unclear. Although possibly the signature of a highly asymmetrical supernova explosion, the remnant’s pinched expansion near the east-west band of high helium abundance filaments (MacAlpine et al. 1989; Lawrence et al. 1995; Satterfield et al. 2012) and the synchrotron’s east and west ‘bays’ (Fesen et al. 1992) may be indicators of circumstellar material that impeded the expansion (MacAlpine et al. 1989; Fesen et al. 1997; Smith 2003, 2013). While the presence of a pre-SN circumstellar material has also been proposed to help explain both the early and late optical luminosity of the Crab supernova (Sollerman et al. 2001; Smith 2013) (but see Moriya et al. 2014 for an alternative view), the existence of any pre-SN circumstellar material around the Crab has not been firmly established (Michel et al. 1991; Hester et al. 1995; Hester

2008).

6. CONCLUSIONS

The Crab’s lone, cylindrical-like ‘jet’ feature along its northern limb has presented a puzzle ever since its discovery in 1970. Although faint, its $100''$ length in a remnant whose radius is less than $200''$ makes it a significant feature in the remnant’s overall structure and deserves to be understood.

Our moderate resolution [O III] spectra and 3D reconstructions offer the most detailed look to date at the kinematic and overall structure of the jet and its interface with the rest of the nebula. From analyses of these data, we find the following:

1) The jet’s systemic velocity is $+170 \pm 15 \text{ km s}^{-1}$ with radial velocities ranging from -190 to $+480 \text{ km s}^{-1}$ and transverse velocities of 1600 to 2650 km s^{-1} from base to tip. The jet consists of thin filamentary walls ($V_{exp} \simeq 40 - 75 \text{ km s}^{-1}$), is virtually hollow of [O III] emission, and elliptical in shape. Increasing radial velocities of the red and blue sides of the jet over its length indicate a funnel-like structure rather than a cylindrical tube as previously thought.

2) The jet’s blueshifted facing and redshifted rear sides are relatively well defined and appear in rough alignment with the remnant’s center of expansion. Such radial alignments suggest a causal connection between the jet’s formation and the Crab’s expansion point and do not support jet formation models invoking a post supernova rupture in the expanding shell of debris along the Crab’s northern limb, or energy flow off the pulsar toward this region.

3) We find a large and nearly emission-free opening in the remnant’s thick outer ejecta and shell located directly below the jet and along the northernmost point of the Crab’s north bipolar expansion. The jet’s position at the top of the bipolar expansion and over this opening strongly suggests the jet to be part of the Crab’s N-S bipolar expansion structure.

Thus, despite an oddly non-radial and parallel walled appearance, when considered in the context of the Crab Nebula’s bipolar expansion structure, its origin seems less mysterious. With an estimated age coincident with the 1054 supernova event, a location atop the remnant’s northern expansion bubble over a large opening in the nebula’s ejecta shell, and a radial funnel-like structure, the jet’s origin seems directly linked to the remnant’s radial expansion. The lack of a similar opening seen in the remnant’s ejecta shell in the Crab’s southern expansion bubble may explain the lack of an opposing jet-like feature along the Crab’s southern limb.

The authors wish to thank Mike Shull and Dan Milisavljevic for providing useful comments and suggestions, and the staff of MDM Observatory for their assistance in making these observations possible. This work has made use of the NASA Astrophysics Data System. RAF’s supernova remnant research is supported by the National Science Foundation under grant No. AST-0908237.

REFERENCES

- Benford, G. 1984, *ApJ*, 282, 154
 Bietenholz, M. F., & Kronberg, P. P. 1990, *ApJ*, 357, L13
 Blandford, R. D., Kennel, C. F., McKee, C. F., & Ostriker, J. P. 1983, *Nature*, 301, 586
 Bühler, R., & Blandford, R. 2014, *Reports on Progress in Physics*, 77, 066901
 Bychkov, K. V. 1975, *Soviet Ast.*, 18, 420
 Chevalier, R. A., & Gull, T. R. 1975, *ApJ*, 200, 399
 Clark, D. H., Murdin, P., Wood, R., et al. 1983, *MNRAS*, 204, 415
 Cocke, W. J., Disney, M. J., & Taylor, D. J. 1969, *Nature*, 221, 525
 Comella, J. M., Craft, H. D., Lovelace, R. V. E., & Sutton, J. M. 1969, *Nature*, 221, 453
 Davidson, K. 1987, *AJ*, 94, 964
 Davidson, K., & Fesen, R. A. 1985, *ARA&A*, 23, 119
 Dombrovski, V. A. 1954, *Doklady Akad Nauk SSSR*, 94, 21
 Duyvendak, J. J. L. 1942, *PASP*, 54, 91
 Fesen, R., & Gull, T. 1983, in *IAU Symposium*, Vol. 101, *Supernova Remnants and their X-ray Emission*, ed. J. Danziger & P. Gorenstein, 145

- Fesen, R. A., & Gull, T. R. 1986, *ApJ*, 306, 259
- Fesen, R. A., Martin, C. L., & Shull, J. M. 1992, *ApJ*, 399, 599
- Fesen, R. A., Shull, J. M., & Hurford, A. P. 1997, *AJ*, 113, 354
- Fesen, R. A., & Staker, B. 1993, *MNRAS*, 263, 69
- Gull, T. R., & Fesen, R. A. 1982, *ApJ*, 260, L75
- Hester, J. J. 2008, *ARA&A*, 46, 127
- Hester, J. J., Scowen, P. A., Sankrit, R., et al. 1995, *ApJ*, 448, 240
- Hester, J. J., Mori, K., Burrows, D., et al. 2002, *ApJ*, 577, L49
- Hubble, E. P. 1928, Leaflet of the Astronomical Society of the Pacific, 1, 55
- Kaplan, D. L., Chatterjee, S., Gaensler, B. M., & Anderson, J. 2008, *ApJ*, 677, 1201
- Kundt, W. 1983, *A&A*, 121, L15
- Lawrence, S. S., MacAlpine, G. M., Uomoto, A., et al. 1995, *AJ*, 109, 2635
- Loll, A. M., Desch, S. J., Scowen, P. A., & Foy, J. P. 2013, *ApJ*, 765, 152
- Lundmark, K. 1938, in Professor Östen Bergstrand Vetenskapsmannen Och Läraren, 89
- Lundqvist, P., & Tziamtzis, A. 2012, *MNRAS*, 423, 1571
- MacAlpine, G. M., McGaugh, S. S., Mazzarella, J. M., & Uomoto, A. 1989, *ApJ*, 342, 364
- Marcelin, M., Veron-Cetty, M. P., Woltjer, L., et al. 1990, *A&A*, 228, 471
- Michel, F. C. 1985, *ApJ*, 288, 138
- Michel, F. C., Scowen, P. A., Dufour, R. J., & Hester, J. J. 1991, *ApJ*, 368, 463
- Moriya, T. J., Tominaga, N., Langer, N., et al. 2014, *A&A*, 569, A57
- Morrison, P., & Roberts, D. 1985, *Nature*, 313, 661
- Ng, C.-Y., & Romani, R. W. 2004, *ApJ*, 601, 479
- Nugent, R. L. 1998, *PASP*, 110, 831
- Osterbrock, D. E., & Ferland, G. J. 2006, *Astrophysics of Gaseous Nebulae and Active Galactic Nuclei*
- Rudie, G. C., Fesen, R. A., & Yamada, T. 2008, *MNRAS*, 384, 1200
- Sankrit, R., & Hester, J. J. 1997, *ApJ*, 491, 796
- Satterfield, T. J., Katz, A. M., Sibley, A. R., MacAlpine, G. M., & Uomoto, A. 2012, *AJ*, 144, 27
- Shklovskii, I. S. 1953, *Doklady Akad Nauk SSSR*, 90, 983
- Shklovskii, I. S. 1957, *Soviet Ast.*, 1, 690
- Shull, Jr., P., Carsenty, U., Sarcander, M., & Neckel, T. 1984, *ApJ*, 285, L75
- Smith, N. 2003, *MNRAS*, 346, 885
- . 2013, *MNRAS*, 434, 102
- Sollerman, J., Kozma, C., & Lundqvist, P. 2001, *A&A*, 366, 197
- Trimble, V. 1968, *AJ*, 73, 535
- . 1973, *PASP*, 85, 579
- Tziamtzis, A., Schirmer, M., Lundqvist, P., & Sollerman, J. 2009, *A&A*, 497, 167
- van den Bergh, S. 1970, *ApJ*, 160, L27
- Velusamy, T. 1984, *Nature*, 308, 251
- Veron-Cetty, M. P., Veron, P., & Woltjer, L. 1985, *A&A*, 151, 101
- Wallace, B. J., Landecker, T. L., Kalberla, P. M. W., & Taylor, A. R. 1999, *ApJS*, 124, 181
- Wilson, A. S., Samarasingha, N. H., & Hogg, D. E. 1985, *ApJ*, 294, L121
- Wilson, A. S., & Weiler, K. W. 1982, *Nature*, 300, 155
- Woltjer, L., & Veron-Cetty, M.-P. 1987, *A&A*, 172, L7